Design of Low-Cost Synchronous Reluctance Motor with a Surrogate-Assisted Optimization Technique

Syed Abid Ali Shah Bukhari[1]*, Imtiaz Ali Leghari[1], Junaid Iqbal Bhatti[1], Saleem Raza[1], Mohsin Ali Koondhar[1], Irfan Ali Channa[2], Muhammad Usman Keerio[1]

Abstract:

This paper presents the performance of centrifugal pump coupled with synchronous reluctance motor of 24kW. The 4-pole 36 slots induction motor stator has been used for the prototype. The reduction of torque ripple and power losses is the main aim of research. Different arrangement of rotor flux barrier shapes has been tested through finite element analysis method. The rotor optimization is done by varying different parameters are used such as, barrier edge angle, width of flux carriers, flux barriers and shaft diameter. In order to improve the motor performance, the method of particle swarm optimization has been used by generating samples with surrogate assisted optimization technique. Distinct flux barrier shapes and designs have been checked through simulation. For the prototype development, final V-shaped best model is chosen. The proposed rotor shows the excellent performance in terms of reduced torque ripple (27%) and improved average torque (154Nm) in experimental results. The suggested design also has good thermal and mechanical performances with the capability to use in various industrial applications.

Keywords: torque ripple, particle swarm optimization, surrogate based technique, flux barrier, machine design, synchronous reluctance motor, direct drive.

1. Introduction

The construction of transverse-laminated rotor structure of synchronous reluctance motor (SynRM) is attracting the attention by the different users, because of its simple construction, cost, robustness and manufacturing process [1],[2]. Typically, a pumping system is mostly used to couple an induction motor of 1500 rpm with a centrifugal pump but, this system has a lot of disadvantages such as heavy and bulky motor drive system with low energy efficient. In this regard, for high-torque applications, permanent magnet synchronous machines (PMSM) are dominated, but the most important issue is the recycling of these rare-earth metal permanent magnets. Additionally, the cost of magnetic material collectively with demand and supply chain issues is actually preventing these machines from assuming its rightful place as a motor of choice near future. So as the price rate of rare-earth magnets is growing, at the same time their market stability is declining [3]. Thus, a universal satisfactory solution has not been adopted for

[1] Quaid-e-Awam University of Engineering, Science and Technology, Pakistan
[2] Department of Automation, Beijing University of Chemical Technology, Beijing, China
Corresponding Author: abidshah@quest.edu.pk

application of closed coupled centrifugal pumps. After an improvement in electrical drives in 20th century due to enhanced efficiency and fast dynamic response of the drives, the reluctance motors represents a much possible alternatives [4],[5].

The reluctance motors have a unique rotor structure which is arranged from laminated steel and do not use permanent magnet. There is salient rotor and works on the basis of reluctance torque. There are two types of reluctance machine the number one is switched reluctance motor (SRM) and second is synchronous reluctance motor (SynRM). If the stator is of round configuration and fed with AC supply with different phases the machine is called synchronous reluctance machines. If the stator has salient poles structure, the machine is called switched reluctance machine. The SRM has high torque ripple and separate DC input source is required to excite the winding. Whereas SynRM utilize sinsoidally distributed windings as in induction or synchronous machines and requires easily available universal sinusoidal supply, so that's why author has decided to take SynRM for the research.

Many industrial applications require low torque ripple, therefore lots of studies have been conducted and to enhance the performance of the machine, like in [6],[7],[8],[9], the torque ripple is investigated and multiple solutions are tested. Further to enhance the torque density of the machine, the rotor design is investigated in [10],[3],[11] in which the saliency ratio is examined which denotes the ratio between the d-axis and q- axis.

For SynRM rotor, the type of axially laminated anisotropy (ALA) is mostly used in a high-speed operation as proved in many research investigations [12-15]. Due to rigid structure and improved saliency ratio [16-18]. However, because of very thicker laminations it produces unwanted flux oscillations with very high iron losses. Therefore, TLA type rotor is most preferable because of simple construction and low losses [19-22]. Hence, due to above advantages of SynRM simulation model design it has been decided to use TLA type rotor. It is aimed to select the
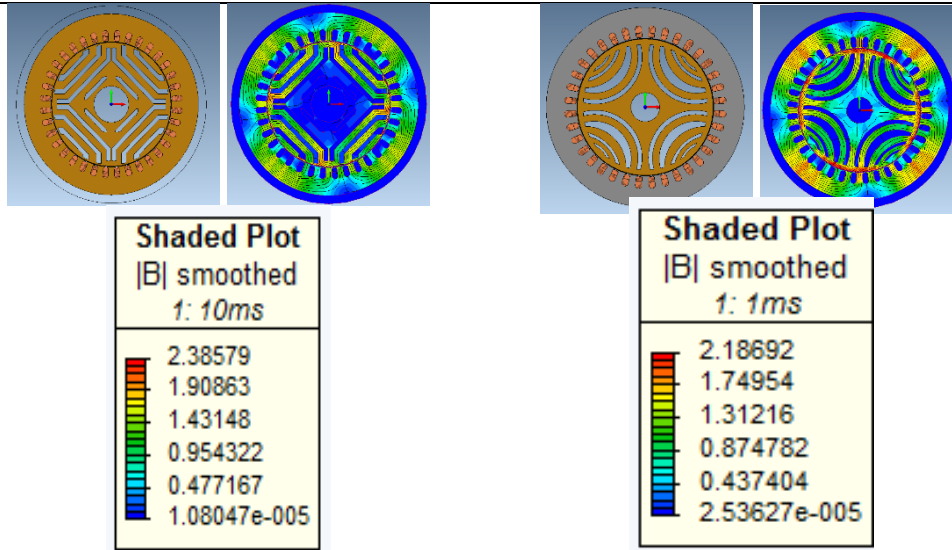
number and shape of flux barriers to achieve the low power losses along with low torque ripples. The paper is distributed in three different sections. The section I describes the background of research.
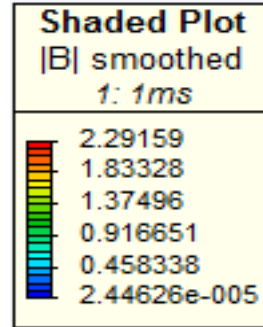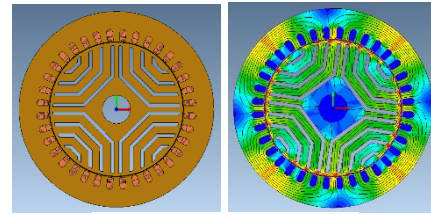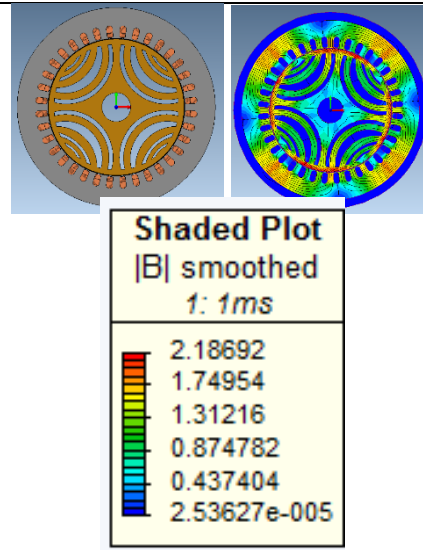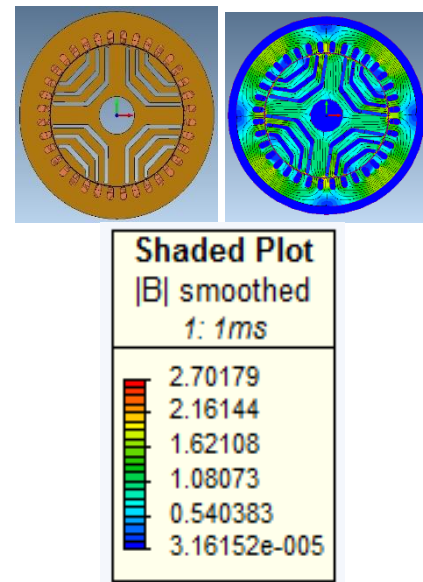

(a)
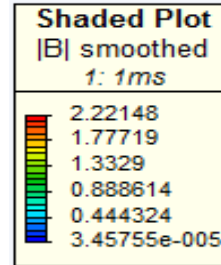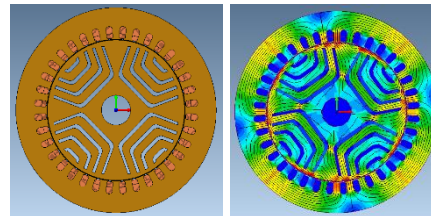
(b)

(c)

Fig 1: Four flux barrier rotor's different designs of SynRM (a) 4 V-shaped flux barrier rotor (b) 4 square shaped rotor (c) 4 straight flux barriers with slight angle at the edges.

(a)

(b)

The detailed rotor design with three and four flux barriers and its advantages have been described through simulation in section II. Also, in order to minimize torque ripple and to enhance efficiency, the analysis on flux barriers and flux carriers carried out by varying the width, and shaft diameter while using Infolytica Magnet software. In section III the development of rotor from manufacturing point of view and its process is mentioned. In order to validate the proposed rotor model, a test bench is set up by manufacturing the designed rotor and the prototype development steps are conducted with the experimental results and discussion with no-load test, low-slip test and Over speed test operation and experimental results of the proposed machine have been described in section IV. In section V, the brief analysis of results has been presented. Finally, section VI describes the research methodologies along with application and future trends.
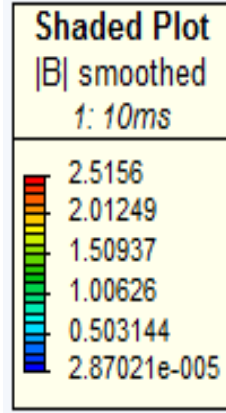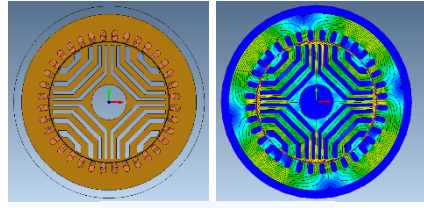
(c)

(d)

Fig 2: Three and four flux barrier rotor designs for SynRM (a) 4 square shaped flux barrier rotor (b) 3 V- shaped rotor (c) 4 square shaped flux barriers with slight angle at the end and 3 square shaped flux barriers.
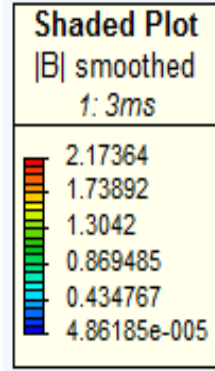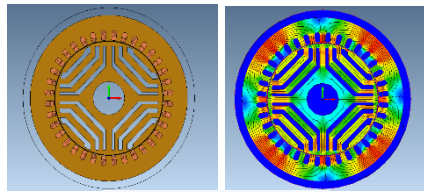
2. Working prniciple of SynRM

In SynRM, to achieve the maximum output, the saliency ratio (Ld-Lq) should be maximized. In this rotor design 0.6 to 0.7 percent saliency ratio has been used. However, the torque is generated through reluctance variation at different rotor positions. The motor torque is directly proportional to the transformation of the magnetizing inductance (d-q axis) which impacts the coordinate system of rotor reference frame. In machine design, the main challenge is to maintain thermal constraints because of stator and rotor windings [23]. Therefore, it is essentially needed to reduce the involvement of winding material and magnetic mass. In [24] a low speed domestic application with direct-drive SynRM having six rotor geometries has been presented. Most of the SynRM employs advanced transversally laminated rotor structure. The rotor cage design is taken out as the machine can be easily started synchronously through inverter control system. Therefore d-q equations of SynRM [25] are established as follows.

$$V_{ds} = r_s\, i_{ds} + \frac{d}{dt} L_{ds}\, i_{ds} - \omega_r\, L_{ds}\, i_{qs} \quad (1)$$

$$V_{qs} = r_s\, i_{qs} + \frac{d}{dt} L_{qs}\, i_{qs} - \omega_r\, L_{ds}\, i_{ds} \quad (2)$$

The Lds and Lqs represents the quadrature and direct axis inductances. The (ωr) is speed, whereas each phase of stator resistance is denoted by (r_s). The electromagnetic torque in terms of d-q variables, is identical to that of a SynRM, namely

$$T_e = \frac{3}{2} \frac{P}{2} \left(L_{ds} - L_{qs} \right) i_{ds}\, i_{qs} \quad (3)$$

Whereas number of poles are denoted by P.
In order to model the asynchronous machine, above equations are used.

3. design and simulation of SynRM

In order to choose the best rotor design, seven different geometries of three and four flux barrier have been examined and finite element analysis carried out. All the test was conducted at 1500RPM as Fig. 1 shows the different flux barrier designs of the rotor. (a)

shows the four flux barriers with V-shaped designs in this design the flux barrier edge angle is kept 49 degree and the torque ripple is 27% which is good but machine efficiency is very low and the total average torque produces by the machine is 134Nm and one additional factor which is the flux density is higher up to 2.29. In design (b) the more angle is provided to sharp edges but the the efficiency reduces to 37% and torque ripple is still higher to 70% and overall average torque is also reducing to 93Nm with flux density 2.2T. In design 132Nm torque is produced with 2.38T flux density and the torque ripple is 42%. In Fig. 2 (a) circular shape with four flux barrier design are tested which gives the efficiency 47% with 118Nm torque and 2.18T whereas, torque ripple is slightly higher 44%. In (b) three V-shaped flux barrier design are tested which produce the highest torque 158Nm with 70% and low torque ripple 30% but flux design is higher 2.7T. The design (c) gives 134Nm torque and 2.5T density and torque ripple is higher upto 46% with 63% efficiency. In (d) three square shaped flux barrier are used which produces 134Nm torque and 47% torque ripple with 2.17T flux density.

4. Development of Synchronous reluctance Motor

Keeping above data analysis in terms of torque, efficiency, torque ripple and flux density in section III, the author decide to take three V-shaped design as a main investigation point due to its higher high efficiency and torque production. Further design variables flux barrier and carrier width with edges and shaft diameter are modified accordingly. Consequently, a 3-flux barrier's rotor of 24kW SynRM with motor has been simulated with the specifications shown in table, I and II.

Fig 3: Design rotor dimensions of SynRM

Table I: 24kW SynRM specifications.

Parameter	Units	Value	Symbol
Number of phases	-	3	*m*
total flux barriers	-	3	-
speed	rpm	1500	*nN*
Number of turns	turns	12	*Np*
Number of stator poles	-	4	*Ns*
frequency	Hz	50	*f*
Rated current	Amps	26	*I*
angle of edges	o	4	*deg*
Rated power	kW	24	*P*
Saliency ratio		0.7	
Phase Voltage	V	380	*Vdc*
Stator diameter	mm	310	*ds*
Air-gap	mm	1	*g*
Machine length	mm	200	*l*
Average torque	Nm	154	*Tav*
diameter	mm	188	*dr*
Shaft diameter	mm	50	*dsh*

Table II. SynRM rotor design Specifications

Item	Value	Item	Value
Rotor Material	M350-50Amp		
carrier width	12.06, 9.92,9.97,10.21	barrier width	9.02, 8.97, 8.81

Overall carrier width	42.17	Overall barrier width	26.822
Rotor OD	188 mm	Flux barrier edge angle	3 and 4 deg
length of first barrier (starting at outer diameter)			
Lower	35.9mm	Upper	36mm
length of second barrier			
Lower	36mm	Upper	36mm
length of third flux barrier			
Lower	35.63mm	Upper	35.91mm

Note: All the dimensions are depicted in rotor's half or 4th quadrant in Fig. 3.

At first four and five barriers with square shaped ware simulated. However, their performance was not reasonable and machine was generating 2.7T magnetic flux density and the produced torque was also low in between (100 to 120Nm). Then configurations of 3 flux barrier were simulated with V-shaped flux barrier design has been proposed, as depicted in fig. 4(a)- and two-dimensional mesh view is shown in Fig. 4(b). The 2.1 Tesla of flux density, current waveform and produced torque is shown in Fig. 5 (a to c) respectively.
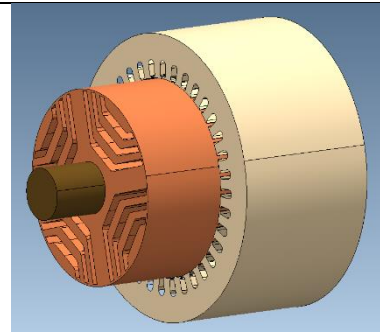

(a)
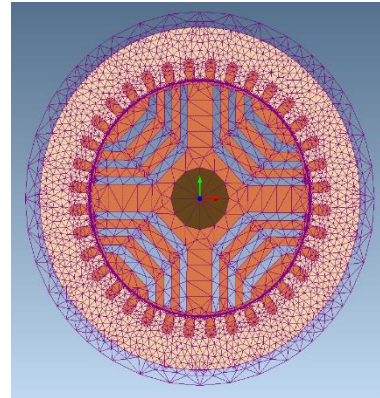
(b)

Fig 4: (a) Model of two dimensional SynRM (b) Triangular view of meshes

At 500 milliseconds transient simulation with velocity-driven settings carried out, thus machine can produce effective starting torque 180 Nm and 154.30Nm average torque with 90% efficiency. The portion of the shaft kept hollow to avoid additional magnetic losses therefore its losses are very negligible, so that's why has author has not considered in this work. the copper, hysteresis and eddy current losses are 2.358watts and the stator hysteresis and eddy current losses are 379watts,
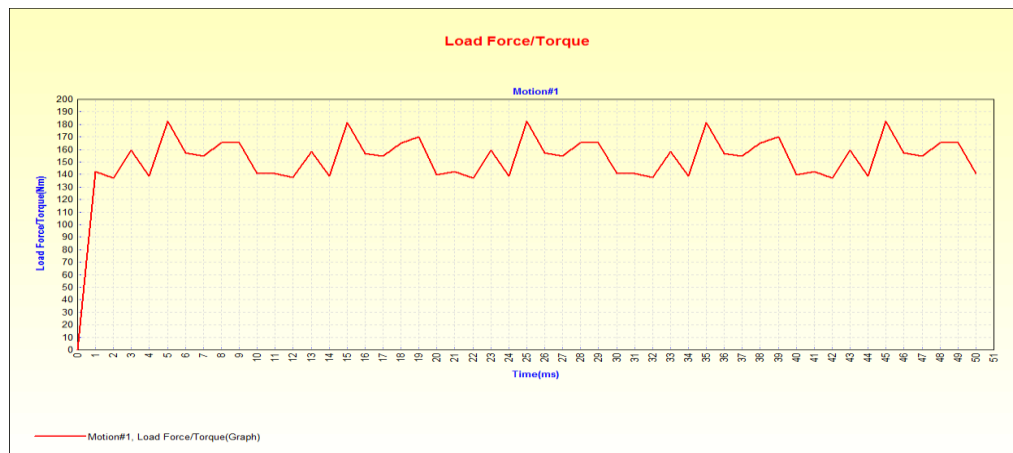
The 1000/65 Newcore nonlinear lamination material selected for the stator and for rotor lamination M350-50A material used in the machine.
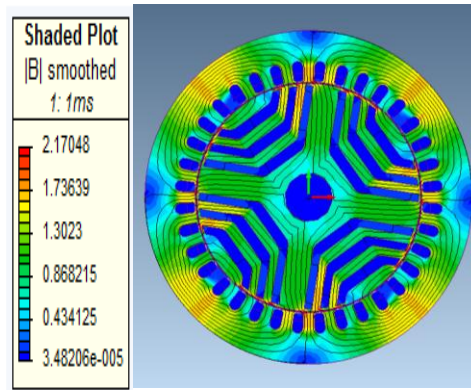
(a)
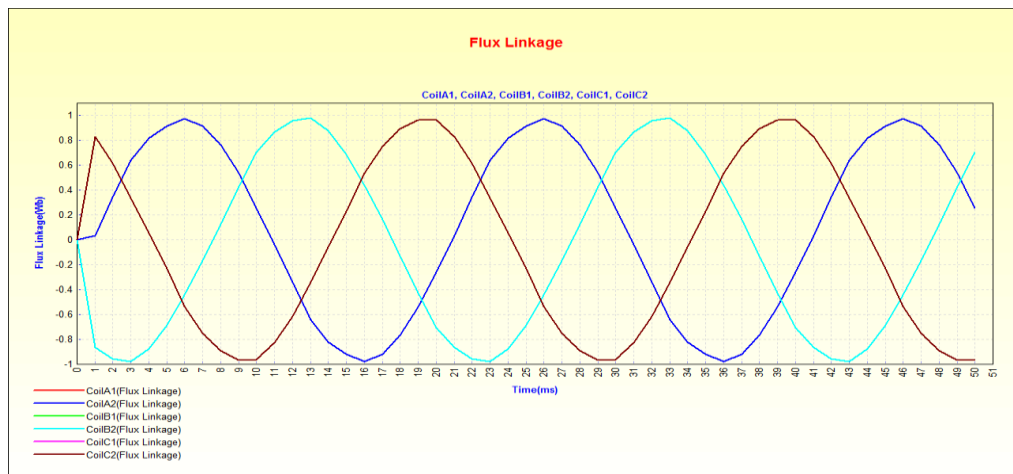
(b)

(c)

Fig. 5 (a) 2.1 (Tesla) flux density (b) Flux linkage (c) generated torque of the SynRM
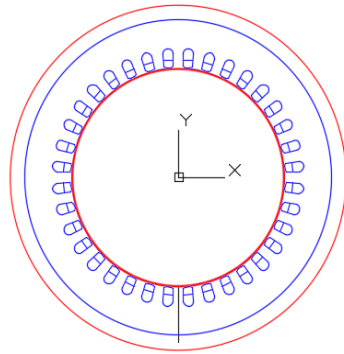
Fig 6: The 4 pole 36 slots double layer stator

5. Experimental Validation

Subsequently the optimization of rotor design scheme the machine performance was examined and the 3-flux barrier rotor design was chosen for further refinement and Surrogate based optimization technique was applied with four main variables of rotor design which are Flux barrier width, flux carrier width, shaft diameter and barrier edge angle. Total 20 Latin hypercube samples are generated to check the toraue, efficiency, torque ripples and magnetic flux density. And finally, best design is selected for the prototype development.

Rotor Fabrication

(a) Early manufacturing and final manufacturing rotor from factory

(b) Flux barrier filling with magic and PVC insertion

(c) Assembled rotor with shaft, fan and bearing before machining

(d) Final assembled rotor after machining

Fig 7: Prototype development stages of the proposed rotor (a) early manufacturing from the factory (b) flux barrier filling with magic and PVC (c) assembled rotor with shaft (d) final assembled rotor after machining

In order to improve the mechanical integrity of the rotor manufacturing process, the polyvinylchloride material was inserted inside of the flux barrier and it took almost 2 days to dry the rotor. The complete rotor manufacturing stages from manufacturing in the factory to assembled rotor in the machining process are shown in Fig. 7. The stator for the proposed motor used is identical of standard Cummins BCI-184F machine is shown in Fig. 8, whereas the complete specifications are described in [26, 27]. There are short-pitched 2/3 winding arrangement with double layer star connection. Each slot area is 144mm2 for individual layer. The experimental test rig of the whole was built and tested as depicted in Fig. 8.

Fig 8: The Standard stator from a Cummins BCI-184F machine

A-NO-LOAD TEST

An experimental set-up was conducted in order to measure the rated voltage, current, power and other parameters at no-load and is shown is Fig. 9. The no load speed test is conducted at 13.3ºC ambient temperature by coupling the shaft of proposed machine with 55kW permanent magnet synchronous machine. The simulation results achieved through the FEM analysis are validated by experimental measurements on the test bench. The designed SynRM was tested under no-load condition, at fifteen different driven speed and ten different frequencies. The frequency varied at steps: 5, 10, 15, 20, 25, 30, 33, 35, 38, 40, 42, 45 and 50. Thus the machine speed has been changing according

to synchronous speed: 150, 299, 452, 600, 752, 900, 995, 1052, 1140, 1200, 1260, 1314, 1350, 1433, 1500 RPM.

Table VII. No-load experimental data of speed, current, voltage, power, power factor, harmonics and vibration from 0-50Hz frequency.

Fig 9: Experimental test rig

A. The SynRM
B. Siemens Drive
C. 55kW load motor
D. ABB Drive
E. Temperature meter
F. Oscilloscope Tektronix TDS 2024B
G. Torque meter JN-338
H. Fluke power meter
I. Mutimeter
J. Speed meter
K. Torque transducer
L. Siemens circuit breaker CDM10-100/3300 Delixi
M. Motor side coupling
N. N. Load side coupling

43.8, 45, 47.8, 50 Hz frequency. Table III presents the rms value of current and voltage with power, power factor, total harmonics distortion and vibration reading at various speed.

Table IV shows the temperature readings at for 150 to 1500 rpm driven speed respectively and Fig. 10. depicts the temperature graph at 5 to 50Hz frequency. As it can be noted that the from no-load test results the number of harmonics and vibration is decreasing as the machine is getting higher

speed mainly due to fact that as the machine's performance becomes more stable. The reduction of harmonics and vibration content is therefore and important achievement in the results.

Table III. No-load Test Temperature experimental data of speed, current, voltage, power, power factor and harmonics from 0-50Hz frequency.

Hz	RPM	I	V	kW	P.f	Harmonics	Vibration m/s^2
5	150	17.8	155	0.28	0.08	254	102.1
10	299	18.3	163.5	0.29	0.09	141.8	99.9
15	452	18.2	172.9	0.36	0.10	165%	98
20	600	18	182	0.34	0.09	116%	99.6
25	752	18	190	0.36	0.10	16.7/0.4/5.3	98.5
30	900	18.1	196.2	0.36	0.10	9.2/6.7/0.3	100
33	995	19.7	199	0.38	0.11	13.6/2.4/14.7	97.2
35	1052	18.2	202	0.40	0.11	8.5/7.5/0.4	97.7
38	1140	18.4	208	0.42	0.11	14.5/12.4/7.1	97.9
40	1200	18.4	213	0.45	0.12	14.3/11.2/	96
42	1260	18.8	217.4	0.52	0.13	8.26%	91.5
43.80	1314	21.7	221	0.53	0.13	8.3/13.7	91
45	1350	18.4	229	0.52	0.13	6.7/4./0.8	92
47.8	1433	18	236	0.55	.13	8.3/13.7	93
50	1500	18.4	249	0.56	0.14	6.4/5.1/0.6	93

B-LOW-SLIP TEST

In order to verify the analysis in the paper, the low slip test is performed. In the low slip test different performance of synchronous reluctance motor carried out, the speed is varied from 150 to 1500rpm by Siemens VFD and the load motor 55kW is rotated anti clockwise at different speed and torque settings and all the parameters are noted such as current, voltage, power, power factor and harmonics. The test machine is derived by Siemens-Micromaster-440 drive and the 55kW coupled machine is derived by ABB ACS800 drive.

The temperature readings along with current, voltage, power, power factor and harmonics are shown in table IV and V, whereas the harmonics reading and parameter setting of load drive motor is shown in table VI.
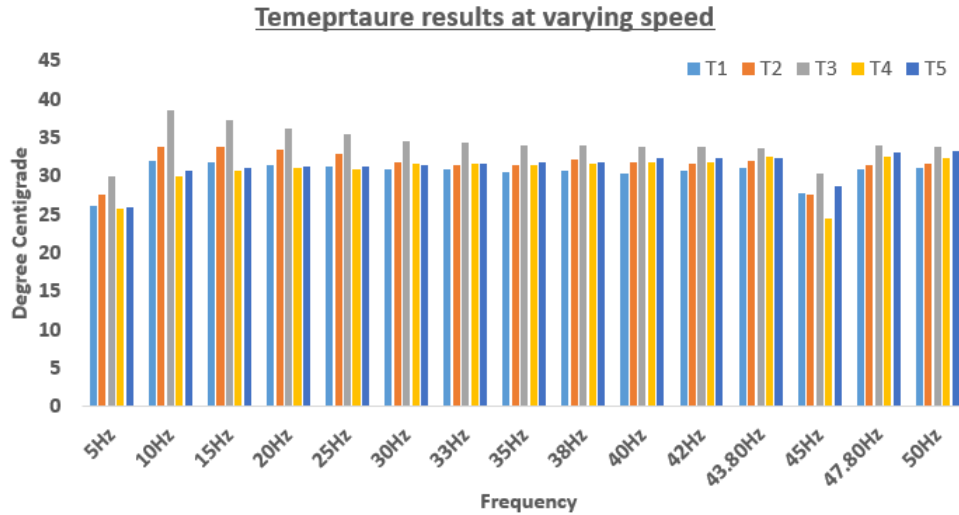
Fig 10: Temperature graph as different input frequency and speed

Table IV. Low-Slip Test Temperature readings of the test machine from 0-50 frequency and 0 to 1500RPM rated speed

Frequency	T1	T2	T3	T4	T5	RPM
5Hz	29.3	30	31.9	32	27.6	150
17Hz	32.3	34.1	37.2	30	31.4	513
25Hz	32.3	34	36.6	31.3	31.8	750
Not Torque applied by ABB at 50Hz						
25Hz	32.8	34.5	36.8	33	32.7	750
30Hz	32.8	34.2	36.7	33.2	33.2	899
Now Torque Applied on the machine						
30Hz	32.7	34.1	36.7	33.4	33.6	900
35Hz	33	34.5	37.1	33.6	34.1	1050
Now Torque Applied on the machine						
35Hz	33.5	34.9	37.5	34.3	34.6	1050
40Hz	34.1	35.2	37.9	34.8	35.7	1200
Now Torque Applied on the machine						
40Hz	34.2	35.2	37.9	34.4	35.9	1200
45Hz	35.4	36.2	39.5	36.2	36.8	1356
Now Torque Applied on the machine						
45Hz	36.1	37	40.2	37.1	37.8	1350
50Hz	36.6	37.7	41.1	37.6	38.3	1500

Table V. Low-slip test

Frequency	RPM	Current	Voltage	Power	P.f
5Hz	150	18	139	0.22	0.09
17Hz	513	18.2	163	0.36	0.12
25Hz	750	17.8	181	41	0.14
	Now Torque applied by ABB at 50Hz				
25Hz	750	18	181	0.51	0.16
30Hz	899	18	192	0.54	0.17
	Now Torque Applied on the machine				
30Hz	900	18.2	191	0.68/0.76	0.21
35Hz	1050	19	312	0.85	0.224
	Now Torque Applied on the machine				
35Hz	1050	18.8	200	0.94	0.25
40Hz	1200	18.9	211	1.10	0.26
	Now Torque Applied on the machine				
Same all	1200	18.9	211	1.10	0.27
45Hz	1356	20.7	227	1.17	0.28
	Now Torque Applied on the machine				
45Hz	1350	20.7	226	1.76	0.37
50Hz	1500	23.8	239	2.29	0.41

Table VI. Harmonics produces by the SynRM and parameter settings of load motor.

Harmonics	Torque Nm	ABB drive reference settings Hz/Rpm	ABB Drive current
512%	0.2	0.1Hz/	
44.7%	0.42	0.6/-9.8	2.4
	0.5	0.6/-9.8	2.9
Not Torque applied by ABB at 50Hz			
14.5/4.9/0.4		0.8/-11.7/-52%	45/6.3
8.3/3.0/0.5	0.9	0.8/-11.7	45/6.3
Now Torque Applied on the machine			
8.5/3.3/0.2	1.4	1/68%	68/10.1
7.5/4.8/0.3	1.7	1.1/-77%	67/11.4
Now Torque Applied on the machine			
7.4/4.2/0.2	1.7	1.2/-16rpm/-84%	72/15
12/8.2/2	2.3	1.2/-16rpm/-84%	72/15
Now Torque Applied on the machine			
12/8.1/0.3	2.3	1.4/-19/99	86/19
7.2/6.3/0.2	2.9	1.4/19.6	84/11.8
Now Torque Applied on the machine			
7.2/6.2/0.3	3.4	1.7/-23.8/117.74T	102.84/12
5.9/6.1/0.3	3.9	1.7/-24.7rpm/-113T	99.74/18

C-OVERSPEED TEST

In order to verify the analysis in the paper, the over speed and test is performed. Firstly, the machine was speedup to normal speed at 1500RM and then gradually speed was increased while varying the frequency from 51-55Hz. It was observed the machine was running good with thermally stable. The experimental results of overspeed test are shown at Table VII and VIII.

Table VII. Low-slip test experimental data of speed, current, voltage, power, power factor and harmonics from 0-50Hz frequency.

Speed Rpm	Frequency	Current	Voltage	Power	P.f	Harmonics
1530	51Hz	1530	18.9	245	0.44	0.15
1560	52Hz	1560	22.5	248	0.63	0.124
1590	53Hz	1590	17.8	249	0.0.59	0.13
1620	54Hz	1620	18.1	251.9	0.65	0.14
1635	54.5Hz	1635	17.3	250	0.64	0.14
1650	55Hz	1650	17.2	251	0.64	0.15

Table VIII. Over speed Test Temperature readings of the test machine from 0-50 frequency and 0 to 1500RPM rated speed.

| Speed Rpm	Frequency	T1	T2	T3	T4	T5
1530	51Hz	29.5	29.6	32.1	23.4	31
1560	52Hz	29.8	30	32.4	27.4	31.7
1590	53Hz	30.2	30.2	32.7	29.2	31.9
1620	54Hz	30.3	30.3	33	31.7	32.2
1635	54.5Hz	30.6	30.8	33	31.3	22.6
1650	55Hz	30.9	30.8	33.1	32.3	32.8

6. Analysis of Experiment Results

The main aim of the experimental validation is to confirm the simulation model at no-load, low slip and over speed test. Addition to this, temperature at different speed of each method is determined. In the over speed test as per Siemens drive default settings machine is started at 5Hz frequency which runs at 150RPM at ambient temperature 16.2 degree centigrade. There are 5 thermocouple temperature sensors have been located at different positions in the test machine.
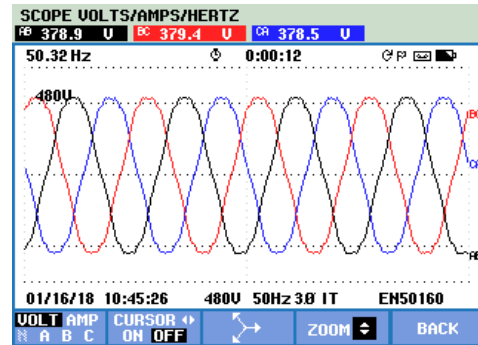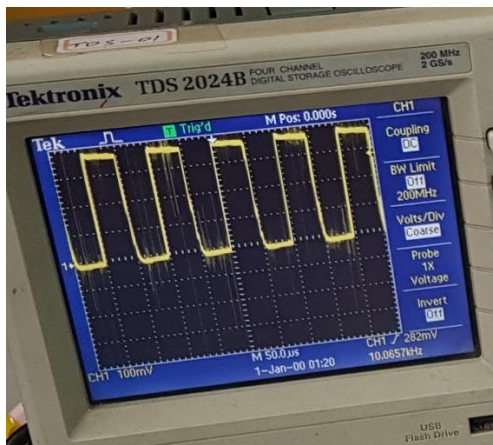

(a)
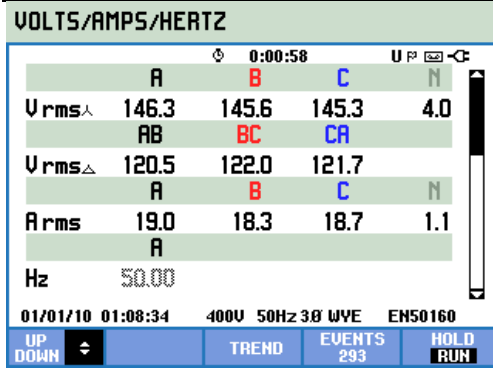
(b)
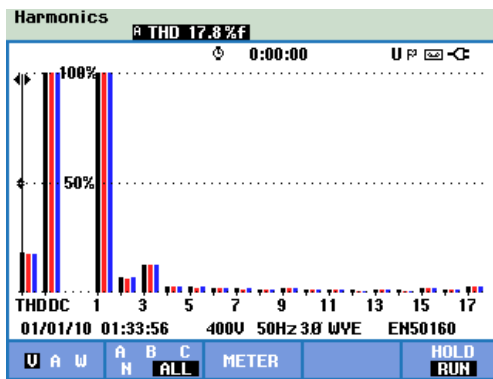
(c)

(d)

Fig.11 Experimental results (a) The voltage wave form; (b) power and power factor reading; (c) total harmonics distortion; (d)

torque wave form at different input frequency and speed

The three sensors are used for winding and their location is 120 mechanical degree apart and two sensors are located at stator outer body. The results of over speed test of all the parameters and temperature parameters are shown in Table VII and VIII respectively. The reading T1, T2 and T3 shows the winding temperature whereas T4 and T5 is the stator outer body temperature. The speed is controlled from the input supply frequency from Siemens drive. It can be observed from the data reading that the T3 has the highest reading 33.1ºC at 15Hz frequency with 1650RPM whereas remaining all the temperature reading is below the maximum which reflects that the machine the thermally stable. The graph of bar chart also depicts the temperature reading under various frequency changes as shown in Fig 10. The no-load experimental data of speed, current, voltage, power, power factor, harmonics and vibration are shown in Table. III and their corresponding photos of 3-phase current wave form, amperes, voltage and frequency values with total harmonics distortion and generated torque wave form are shown in Fig. 11 (a-d). It is observed that initially the machine has high vibration at low speed but as the speed is increased the machine is also stable which is very good in terms of mechanical point of view at can be seen from the data at 50Hz frequency and 1500RPM the vibration is 93 m/s2 which is much better than at the time of starting.

7. Conclusion

This paper has presented the simulation and experimental studies on synchronous reluctance machine with a symmetrical rotor design for centrifugal pumps. A technique based on surrogate with particle swarm optimization has been developed to aid in the machine. Distinct shapes of the rotor are analyzed through simulation and modified the flux barrier shape, shaft diameter and angle of edges to reduce the torque ripple and losses of the machine. The experimental results validate the numerical designs for the proposed machine. A permanent magnet material could also be inserted in rotor flux

barriers to improve flux density. As this would be beneficial for high torque machines. The proposed rotor A symmetrical rotor can improve effective thermal and mechanical performance of the machine and can be beneficial for some applications which are uni-directional in machine operations, as this work is targeted.

References

[1] S. Yammine, C. Henaux, M. Fadel, S. Desharnais, and L. Calégari, Synchronous reluctance machine flux barrier design based on the flux line patterns in a solid rotor," "in *Electrical Machines (ICEM), 2014 International Conference on*, 2014, pp. 297-302.

[2] P. S. Ghahfarokhi, A. Belahcen, A. Kallaste, T. Vaimann, L. Gerokov, and A. Rassolkin, "Thermal Analysis of a SynRM Using a Thermal Network and a Hybrid Model," in 2018 XIII International Conference on Electrical Machines (ICEM), 2018, pp. 2682-2688.

[3] E. Howard, M. J. Kamper, and S. Gerber, "Asymmetric flux barrier and skew design optimization of reluctance synchronous machines," *IEEE Transactions on Industry Applications,* vol. 51, pp. 3751-3760, 2015.

[4] S. Taghavi and P. Pillay, "A sizing methodology of the synchronous reluctance motor for traction applications," *IEEE Journal of Emerging and Selected Topics in Power Electronics,* vol. 2, pp. 329-340, 2014.

[5] A. Boglietti, A. Cavagnino, M. Pastorelli, and A. Vagati, "Experimental comparison of induction and synchronous reluctance motors performance," in *Industry Applications Conference, 2005. Fourtieth IAS Annual Meeting. Conference Record of the 2005*, 2005, pp. 474-479.

[6] R.-R. Moghaddam, F. Magnussen, and C. Sadarangani, "Novel rotor design optimization of synchronous reluctance machine for low torque ripple," in *2012 XXth International Conference on Electrical Machines*, 2012, pp. 720-724.

[7] N. Bianchi, S. Bolognani, D. Bon, and M. Dai PrÈ, "Torque harmonic compensation in a synchronous reluctance motor," *IEEE Transactions on energy conversion,* vol. 23, pp. 466-473, 2008.

[8] M. Sanada, K. Hiramoto, S. Morimoto, and Y. Takeda, "Torque ripple improvement for synchronous reluctance motor using an asymmetric flux barrier arrangement," *IEEE Transactions on Industry Applications,* vol. 40, pp. 1076-1082, 2004.

[9] M. Gamba, G. Pellegrino, and A. Vagati, "Design of non conventional Synchronous Reluctance machine," 2018.

[10] D. Staton, T. Miller, and S. Wood, "Maximising the saliency ratio of the synchronous reluctance motor," in *IEE Proceedings B (Electric Power Applications)*, 1993, pp. 249-259.

[11] M. Kamper and A. Volsdhenk, "Effect of rotor dimensions and cross magnetisation on Ld and Lq inductances of reluctance synchronous machine with cageless flux barrier rotor," *IEE Proceedings-Electric Power Applications,* vol. 141, pp. 213-220, 1994.

[12] J. Ikaheimo, J. Kolehmainen, T. Kansakangas, V. Kivela, and R. R. Moghaddam, "Synchronous high-speed reluctance machine with novel rotor construction," *IEEE Transactions on Industrial Electronics,* vol. 61, pp. 2969-2975, 2014.

[13] M. E. H. Zaim, "High-speed solid rotor synchronous reluctance machine design and optimization," *IEEE Transactions on Magnetics,* vol. 45, pp. 1796-1799, 2009.

[14] H. Hofmann and S. R. Sanders, "High-speed synchronous reluctance machine with minimized rotor losses," *IEEE Transactions on Industry Applications,* vol. 36, pp. 531-539, 2000.

[15] Y. Gessese and A. Binder, "Axially slitted, high-speed solid-rotor induction motor technology with copper end-rings," in *Electrical Machines and Systems, 2009. ICEMS 2009. International Conference on*, 2009, pp. 1-6.

[16] I. Boldea, Z. Fu, and S. Nasar, "Performance evaluation of axially-laminated anisotropic (ALA) rotor reluctance synchronous motors," *IEEE transactions on industry applications,* vol. 30, pp. 977-985, 1994.

[17] D. Platt, "Reluctance motor with strong rotor anisotropy," in Industry *Applications Society Annual Meeting, 1990., Conference Record of the 1990 IEEE*, 1990, pp. 224-229.

[18] D. Platt, "Reluctance motor with strong rotor anisotropy," *IEEE transactions on industry applications,* vol. 28, pp. 652-658, 1992.

[19] M. J. Kamper, F. Van der Merwe, and S. Williamson, "Direct finite element design optimisation of the cageless reluctance synchronous machine," *IEEE*

Transactions on Energy Conversion, vol. 11, pp. 547-555, 1996.

[20] S. Taghavi and P. Pillay, "A mechanically robust rotor with transverse-laminations for a synchronous reluctance machine for traction applications," in *Energy Conversion Congress and Exposition (ECCE), 2014 IEEE*, 2014, pp. 5131-5137.

[21] S. M. Taghavi and P. Pillay, "A mechanically robust rotor with transverse laminations for a wide-speed-range synchronous reluctance traction motor," *IEEE Transactions on Industry Applications,* vol. 51, pp. 4404-4414, 2015.

[22] J. Kostko, "Polyphase reaction synchronous motors," *Journal of the American Institute of Electrical* Engineers, vol. 42, pp. 1162-1168, 1923.

[23] A. A. S. Bukhari, S. Ali, S. H. Shaikh, T. A. Soomro, Z. Lin, and W. Cao, "Design of a high speed 18/12 switched reluctance motor drive with an asymmetrical bridge converter for electric vehicles," in *Computing, Mathematics and Engineering Technologies (iCoMET),*

2018 International Conference on, 2018, pp. 1-6.

[24] M. A. Raj and A. Kavitha, "Effect of Rotor Geometry on Peak and Average Torque of External Rotor Synchronous Reluctance Motor (Ex-R SynRM) in comparison with Switched Reluctance Motor for Low Speed Direct Drive Domestic Application," *IEEE Trans. Ind. Appl,* vol. 53, 2015.

[25] T. Matsuo and T. A. Lipo, "Rotor design optimization of synchronous reluctance machine," *IEEE Transactions on Energy Conversion,* vol. 9, pp. 359-365, 1994.

[26] N. Yang, W. Cao, Z. Liu, Z. Tan, Y. Zhang, S. Yu, *et al.*, "Novel asymmetrical rotor design for easy assembly and repair of rotor windings in synchronous generators," in *Magnetics Conference (INTERMAG), 2015 IEEE*, 2015, pp. 1-1.

[27] T. Yuan, N. Yang, W. Zhang, W. Cao, N. Xing, Z. Tan, *et al.*, "Improved Synchronous Machine Rotor Design for the Easy Assembly of Excitation Coils Based on Surrogate Optimization," *Energies,* vol. 11, p. 1311, 2018.